Hindawi
Advances in Civil Engineering
Volume 2019, Article ID 1806532, 11 pages
https://doi.org/10.1155/2019/1806532

Research Article

Tension Test for Axially Vibrated Prestressing Fine-Rolled Screw-Threaded Steel Bars Based on Thread-Contact Connection

Xingu Zhong,[1] **Tianyu Zhang**,[1] **Chao Zhao**,[1] **Xiaojuan Shu**,[1] **Mingyan Shen**,[1] **and Yohchia Frank Chen**[2]

[1]*Hunan Provincial Key Laboratory of Structural Engineering for Wind Resistant and Vibration Control, Hunan University of Science and Technology, Xiangtan 411201, China*
[2]*Department of Civil Engineering, The Pennsylvania State University, Middletown, PA 17057, USA*

Correspondence should be addressed to Xingu Zhong; 464397070@qq.com

Received 15 November 2018; Accepted 28 February 2019; Published 19 March 2019

Academic Editor: Luigi Di Sarno

The interface between anchor plate and anchorage nut can be considered as a coupling spring whose stiffness is essentially the contact stiffness related to normal force at the contact surface, thus removing the usual assumption of fixed connection. The nut threads and steel bar are also connected with a coupling spring with the stiffness determined based on the threads treated as cantilever components. An analytical model was developed to assess the axial vibration of an anchorage system consisting of prestressing fine-rolled screw-threaded steel bars (P/S FSSBs). Both laboratory model and field tests show that the contact stiffness between anchor plate and anchorage nut has good a linear relationship with the effective tension of prestressed tendons. The vibration model was used to obtain the natural frequency and tensile force of a P/S FSSB. It is shown to be feasible and practical. According to the analytical model and test method presented in this paper, the proposed tension tester for P/S FSSBs possesses the features of repeated use, rapid testing, and minimized impact on the construction and is thus suggested for wider practical applications.

1. Introduction

Prestressing fine-rolled screw-threaded steel bars (P/S FSSBs) have been extensively used as vertical prestressing tendons in concrete bridges. The FSSB anchorage system consists of a FSSB, anchor plate with nut at the top and bottom, and exposed segment at the top, as shown in Figure 1 where the anchor plate and anchorage nut are in contact with each other and the nut anchorage section is connected with the FSSB through the threads. The effective tension of the FSSB affects bridge's safety and durability significantly. The exposed section of vertical P/S FSSB including the nut section has been analyzed as a fully fixed cantilever beam by Zhong et al. [1], in which a developed test method was used to measure the effective tension of the bar system by observing the natural frequency change in the exposed section. However, their proposed method would result in a gross error when the tension is low and thus the tensile testing cannot be continued once the exposed section is cut. Therefore, it is necessary to establish a better model to more accurately measure the tensile force in P/S FSSB.

Figure 2 shows the proposed mechanical model representing the FSSB anchorage system (Figure 1). The anchor plate-anchorage nut interface can be represented by a spring with the normal contact stiffness k. The interaction between the threads in the anchorage nut and the FSSB can also be represented by springs with the stiffness k_{st} (see the enlarged view A in Figure 2). Each FSSB end is fixed with the anchor plate and attached to the concrete web of the prestressed concrete (PC) box-girder bridge. The acceleration sensor was installed vertically on the top nut surface and was connected to the signal analyzer, as shown in Figure 2. At the top of the FSSB exposed section, the transient excitation was applied to simulate vibration signals which can then be used to estimate the axial vibration natural frequencies of the bar by a signal analysis. It is possible to estimate the contact stiffness k value based on its relation with the axial vibration natural frequency. Based on proportional relation between contact stiffness k and normal contact force (i.e., the effective tension in P/S FSSB) [2–4], the effective tension in P/S FSSB may be determined indirectly. The model presented in Figure 2 is

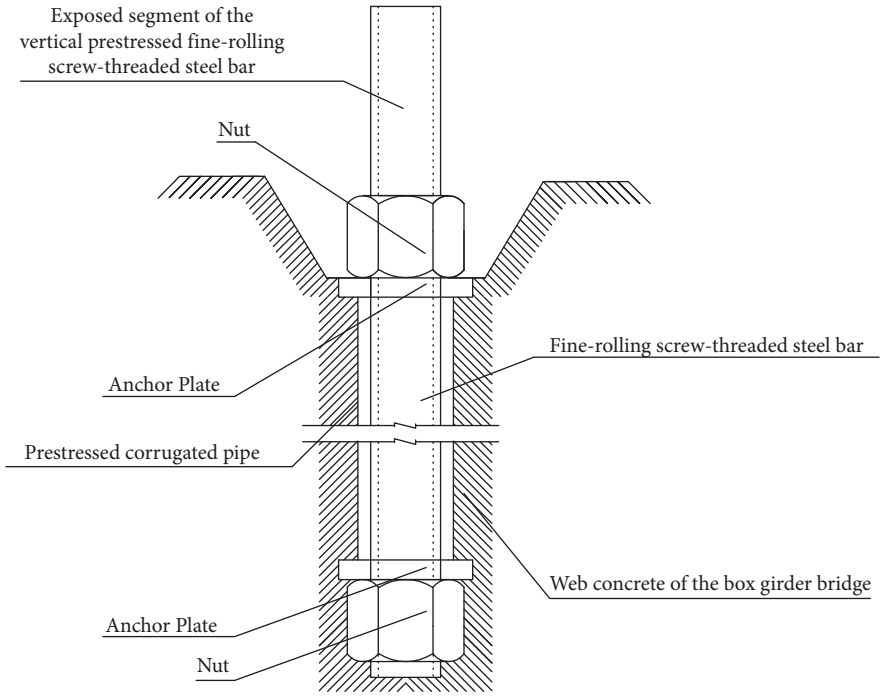

Figure 1: Schematic diagram of a vertical P/S FSSB system.

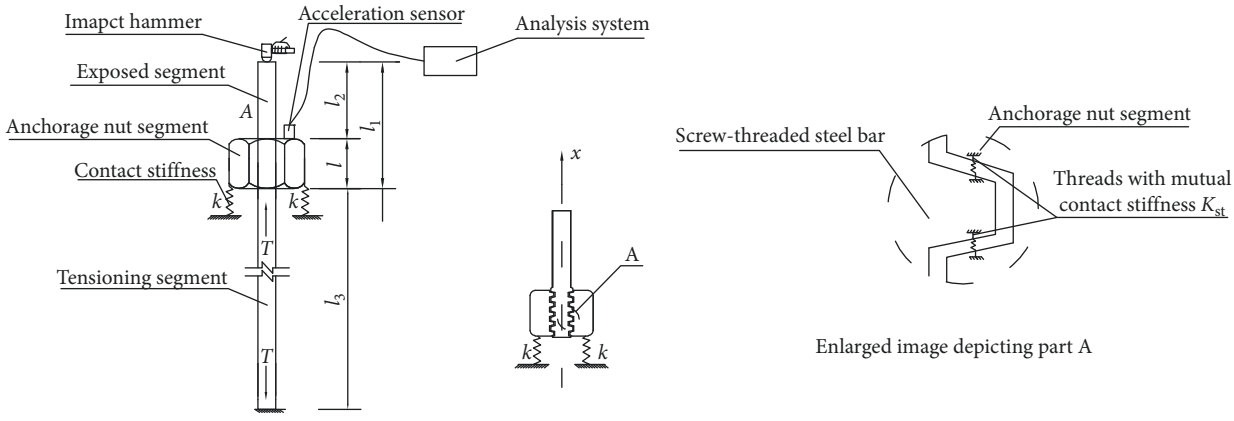

Figure 2: Mechanical vibration model of the vertical P/S FSSB.

similar to the bolt fastening component used in mechanical engineering and pipeline engineering. The relationship between the axial vibration frequency of the mud recovery pipe of deep-water drilling rig and the water depth was studied by Wang et al. [5]. Yang et al. [6] studied the axial vibration control of ship propulsion shafting based on the mass and spring model. An approximate analytical model for the axial vibration of an induction motor was established by Medoued et al. [7], where the acceleration sensor was used to measure axial vibration signals, to analyze the change of axial vibration frequencies, and to realize the damage identification of the motor. Based on the deformation between screw rod and nut threads, a discrete model was developed to evaluate the axial vibration characteristics of a bolt fastener in a variety of mechanical connections [8–11]. 144 experiments were conducted by Tian et al. [3] to estimate the tangential and normal contact stiffnesses at the interface where transient excitations were used to estimate the natural frequencies. Using the springs to represent the contact surface (similar to Figure 2), an analytical model was developed to estimate the tangential and normal stiffnesses at the interface for different normal stress conditions [2–4]. Based on the literature review, it is deemed feasible to obtain the natural frequency to determine the normal contact stiffness by means of exercising transient excitations on the structure with similar contact surface.

2. Discrete Mechanical Model for Axial Vibration

The discrete mechanical model relies on the contacting relationships between the anchor plate and anchorage nut and between the nut threads and FSSB.

2.1. Equations of Motion. Based on Figure 2, a discrete P/S FSSB anchorage system model was developed (Figure 3) in

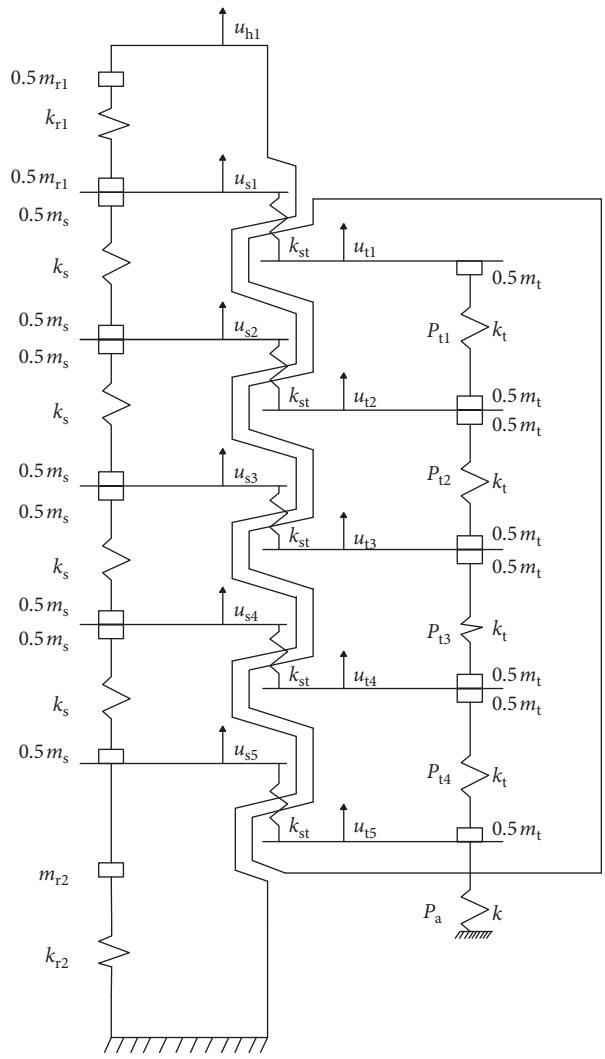

Figure 3: Developed model for discrete mechanical vibration.

which the exposed section l_2 of vertical P/S FSSB (Figure 2) consists of two mass blocks with the mass $0.5m_{r1}$ for each, which are connected by a coupling spring with the stiffness k_{r1} (Figure 3). Note that $m_{r1} = \rho l_2 A$, where A is the cross-sectional area and ρ is the mass density of FSSB. The tensioning section l_3 of vertical P/S FSSB (Figure 2) consists of a mass block with the mass m_{r2} and a coupling spring with the stiffness k_{r2} (Figure 3), where $m_{r2} = \rho l_3 A$. The object of this study is the anchorage system in which the anchorage nut has four laps of threads [12]. The anchorage nut section l (Figure 2) and each lap of threads in the anchorage nut are discretized into two mass blocks with the masses $0.5m_s$ and $0.5m_t$ and two coupling springs with the stiffnesses k_s and k_t (Figure 3). Note that $m_s = \rho Al/4$ and m_t equals to 1/4 of the mass of the anchorage nut. Each lap of threads and the anchorage nut are connected by a spring with the stiffness k_{st} (see the enlarged view A in Figure 2). It is assumed that the bottom of the anchorage nut section is fixed. u_{h1} is the deformation of the exposed segment; u_{s1}, u_{s2}, u_{s3}, u_{s4}, and u_{s5} are the screw-thread displacements of the FSSB in the anchor section; and u_{t1}, u_{t2}, u_{t3}, u_{t4}, and u_{t5} are the counterparts of the nut (Figure 3). Regarding the studied problem, there is virtually no damping effect, and therefore, it is ignored. The equations of motion for the discrete model shown in Figure 3 can be derived using D'Alembert's principle as follows:

$$0.5m_{r1}\ddot{u}_{h1} + k_{r1}u_{h1} - k_{r1}u_{s1} = 0, \tag{1}$$

$$0.5(m_{r1} + m_s)\ddot{u}_{s1} - k_{r1}u_{h1} + (k_{r1} + k_s + k_{st})u_{s1} - k_s u_{s2} - k_{st}u_{t1} = 0, \tag{2}$$

$$m_s\ddot{u}_{s2} - k_s u_{s1} + (2k_s + k_{st})u_{s2} - k_s u_{s3} - k_{st}u_{t2} = 0, \tag{3}$$

$$m_s\ddot{u}_{s3} - k_s u_{s2} + (2k_s + k_{st})u_{s3} - k_s u_{s4} - k_{st}u_{t3} = 0, \tag{4}$$

$$m_s\ddot{u}_{s4} - k_s u_{s3} + (2k_s + k_{st})u_{s4} - k_s u_{s5} - k_{st}u_{t4} = 0, \tag{5}$$

$$0.5(m_{r2} + m_s)\ddot{u}_{s5} + (k_{r2} + k_s + k_{st})u_{s5} - k_s u_{s4} - k_{st}u_{t5} = 0, \tag{6}$$

$$0.5m_t\ddot{u}_{t1} + (k_t + k_{st})u_{t1} - k_t u_{t2} - k_{st}u_{s1} = 0, \tag{7}$$

$$m_t\ddot{u}_{t2} - k_t u_{t1} + (2k_t + k_{st})u_{t2} - k_t u_{t3} - k_E u_{s2} = 0, \quad (8)$$

$$m_t\ddot{u}_{t3} - k_t u_{t2} + (2k_t + k_{st})u_{t3} - k_t u_{t4} - k_{st} u_{s3} = 0, \quad (9)$$

$$m_t\ddot{u}_{t4} - k_t u_{t3} + (2k_t + k_{st})u_{t4} - k_t u_{t5} - k_{st} u_{s4} = 0, \quad (10)$$

$$0.5m_t\ddot{u}_{t5} + (k + k_t + k_{st})u_{t5} - k_E u_{t4} - k_{st} u_{s5} = 0. \quad (11)$$

In equations (1)–(11), the second-order derivatives of the displacement with respect to time are $\ddot{u}_{h1}$, $\ddot{u}_{s1}$, $\ddot{u}_{s2}$, $\ddot{u}_{s3}$, $\ddot{u}_{s4}$, $\ddot{u}_{s5}$, $\ddot{u}_{t1}$, $\ddot{u}_{t2}$, $\ddot{u}_{t3}$, $\ddot{u}_{t4}$, and $\ddot{u}_{t5}$. The matrix form is

$$\mathbf{M}\ddot{\mathbf{U}} + \mathbf{K}\mathbf{U} = \mathbf{0}, \quad (12)$$

where $\mathbf{M}$ (from equation (14)) and $\mathbf{K}$ (from equation (15)) are the mass and stiffness matrices, respectively; $\mathbf{U}$ is the column displacement vector (from equation (13)); $\ddot{\mathbf{U}}$ is the column vector of acceleration; and $\mathbf{0}$ is the zero column vector:

$$\mathbf{U} = \left[\, u_{h1} \;\; u_{s1} \;\; u_{s2} \;\; u_{s3} \;\; u_{s4} \;\; u_{s5} \;\; u_{t1} \;\; u_{t2} \;\; u_{t3} \;\; u_{t4} \;\; u_{t5} \,\right]^{T}, \quad (13)$$

$$\mathbf{M} = \begin{bmatrix} 0.5m_{r1} & 0 & 0 & 0 & 0 & 0 & 0 & 0 & 0 & 0 & 0 \\ 0 & 0.5m_{r1} + 0.5m_s & 0 & 0 & 0 & 0 & 0 & 0 & 0 & 0 & 0 \\ 0 & 0 & m_s & 0 & 0 & 0 & 0 & 0 & 0 & 0 & 0 \\ 0 & 0 & 0 & m_s & 0 & 0 & 0 & 0 & 0 & 0 & 0 \\ 0 & 0 & 0 & 0 & m_s & 0 & 0 & 0 & 0 & 0 & 0 \\ 0 & 0 & 0 & 0 & 0 & 0.5m_{r2} + 0.5m_s & 0 & 0 & 0 & 0 & 0 \\ 0 & 0 & 0 & 0 & 0 & 0 & 0.5m_t & 0 & 0 & 0 & 0 \\ 0 & 0 & 0 & 0 & 0 & 0 & 0 & m_t & 0 & 0 & 0 \\ 0 & 0 & 0 & 0 & 0 & 0 & 0 & 0 & m_t & 0 & 0 \\ 0 & 0 & 0 & 0 & 0 & 0 & 0 & 0 & 0 & m_t & 0 \\ 0 & 0 & 0 & 0 & 0 & 0 & 0 & 0 & 0 & 0 & 0.5m_t \end{bmatrix}, \quad (14)$$

$$\mathbf{K} = \begin{bmatrix} k_{r1} & -k_{r1} & 0 & 0 & 0 & 0 & 0 & 0 & 0 & 0 & 0 \\ -k_{r1} & k_{r1} + k_s + k_{st} & -k_s & 0 & 0 & 0 & -k_{st} & 0 & 0 & 0 & 0 \\ 0 & -k_s & 2k_s + k_{st} & -k_s & 0 & 0 & 0 & -k_{st} & 0 & 0 & 0 \\ 0 & 0 & -k_s & 2k_s + k_{st} & -k_s & 0 & 0 & 0 & -k_{st} & 0 & 0 \\ 0 & 0 & 0 & -k_s & 2k_s + k_{st} & -k_s & 0 & 0 & 0 & -k_{st} & 0 \\ 0 & 0 & 0 & 0 & -k_s & k_{r2} + k_s + k_{st} & 0 & 0 & 0 & 0 & -k_{st} \\ 0 & -k_{st} & 0 & 0 & 0 & 0 & k_t + k_{st} & -k_t & 0 & 0 & 0 \\ 0 & 0 & -k_{st} & 0 & 0 & 0 & -k_t & 2k_t + k_{st} & -k_t & 0 & 0 \\ 0 & 0 & 0 & -k_{st} & 0 & 0 & 0 & -k_t & 2k_t + k_{st} & -k_t & 0 \\ 0 & 0 & 0 & 0 & -k_{st} & 0 & 0 & 0 & -k_t & 2k_t + k_{st} & -k_t \\ 0 & 0 & 0 & 0 & 0 & -k_{st} & 0 & 0 & 0 & -k_t & k_t + k_{st} + k \end{bmatrix}. \quad (15)$$

2.2. Model Parameters

2.2.1. Stiffnesses of Anchorage Nut and FSSB. It is assumed that the cross-sectional areas of FSSB and anchorage nut before and after the tension are virtually unchanged. In equations (1)–(11), $k_{r1} = \pi d_v^2 E_b/4l_2$, $k_{r2} = \pi d_v^2 E_b/4l_3$, $k_s = \pi d_v^2 E_b/l$, and $k_t = 4A_t E_b/l$, where d_v, l_3, l_2, and l represent the nominal diameter of FSSB, the length of the tensioning section, the length of the exposed section, and the height of the anchorage nut section, respectively. A_t is the area of the cross section of the anchorage nut, and E_b is the modulus of elasticity of FSSB and anchorage nut.

2.2.2. Calculation of the Interaction Stiffness of Threads. Figure 4 shows the anchorage nut and steel bar sections, where d_t, d_s, and d_v are the anchorage nut diameter, screw-thread outer diameter, and nominal diameter of FSSB, respectively. The screw-thread structure is shown in Figure 5 where l_e, l_z, l_p, h, λ, and ϕ are, respectively, the thread pitch, thread lap length, bottom thread width, thread height, tilting angle on the top thread surface, and tilting angle on the bottom thread surface. Treating the threads as cantilever components similarly to the study of Zhong et al. [13], the stiffness of thread interaction between the FSSB and the anchorage nut can be determined by

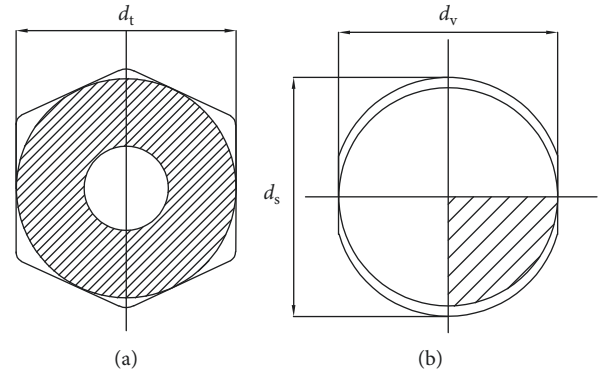

Figure 4: Diagrams showing the cross section of (a) anchorage nut and (b) steel bar.

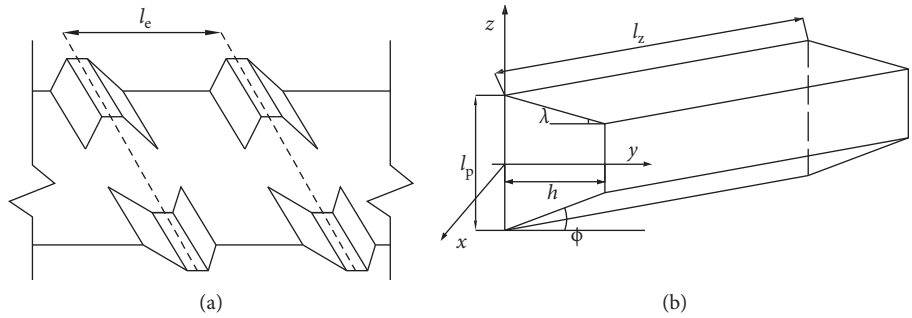

Figure 5: (a) Diagram and (b) enlarged view of the screw-thread structure.

$$k_{st} = \frac{\pi d_s h E_b}{3(E+F+H+I)}, \tag{16}$$

where

$$E = \left(h^3 - \frac{l_p^3}{4} + \frac{10hl_p^2}{8} - 2h^2 l_p\right)\frac{\left(2l_p h - h^2\right)}{l_p^2\left(l_p - h\right)^2},$$

$$F = \left(2h^2 - \frac{5hl_p}{2} + l_p^2\frac{3}{4}\right)\frac{2h}{l_p\left(l_p - h\right)}, \tag{17}$$

$$H = \frac{5h - 3l_p}{4}\ln\frac{\left(l_p - h\right)}{l_p},$$

$$I = \frac{h}{8}.$$

Once relevant calculation parameters are obtained, the following equation can be concluded from equation (12):

$$\left(\mathbf{K} - \omega^2\mathbf{M}\right)\mathbf{U} = \mathbf{0}, \tag{18}$$

where ω is the system's natural frequency.

The nontrivial solution of equation (18) is obtained under the following condition:

$$\left|\mathbf{K} - \omega^2\mathbf{M}\right| = \mathbf{0}. \tag{19}$$

The unknown parameters in equation (19) include the natural vibration frequency ω and the contact stiffness k. If ω is found, k can be obtained from equation (19) and then the natural vibration frequencies of each mode can be determined for the model shown in Figure 2.

3. Experimental Investigation on the Natural Frequency-Tension Relationship of FSSB under Axial Vibration

3.1. Modeling and Test Scheme. The test model was a reinforced concrete (RC) cuboid with the strength grade of C50 and the dimensions of 300 cm × 360 cm × 120 cm. In the model, reserve double row ducts with five 5 cm diameter ducts spaced at ≈45 cm in each row were used. The compression bars and anchor plate of Q235 were set at both ends of the duct before pouring the concrete. The FSSB with the diameter of 32 mm and its anchoring system were used in this test. This experiment used five additional steel bars with the respective tension values of 100 kN, 200 kN, 300 kN, 400 kN, and 530 kN. Figure 6 shows the experimental model of this study.

In order to ensure that the frequency test and analysis are not affected by boundary conditions, the P/S FSSB was not installed with the force sensor. To measure the effective tension similarly to the study of Zhong et al. [14], the test device shown in Figure 7 was used. The test scheme was set up as follows: (1) first, the anchorage nut was installed and the vertical P/S FSSB was connected by a connecting sleeve, followed by the installation of the lifting jack, reaction frame,

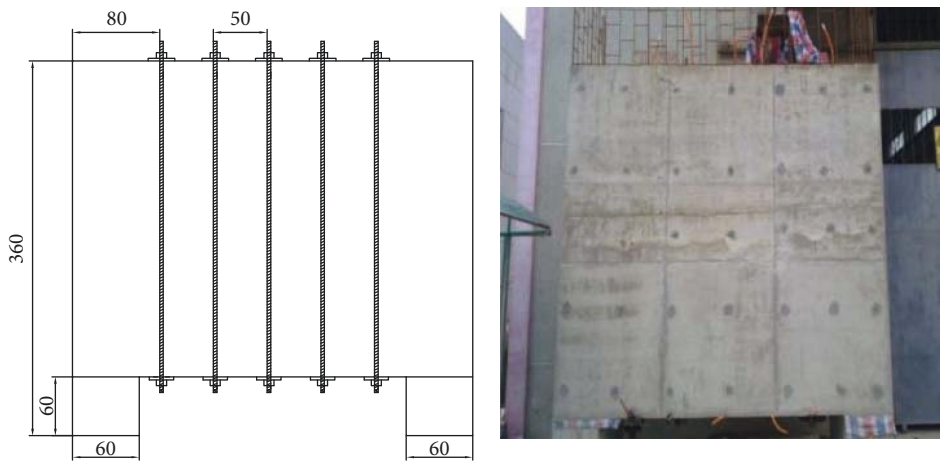

Figure 6: Experimental model developed for vertical P/S FSSB: (a) overall view (unit: cm) and (b) photo.

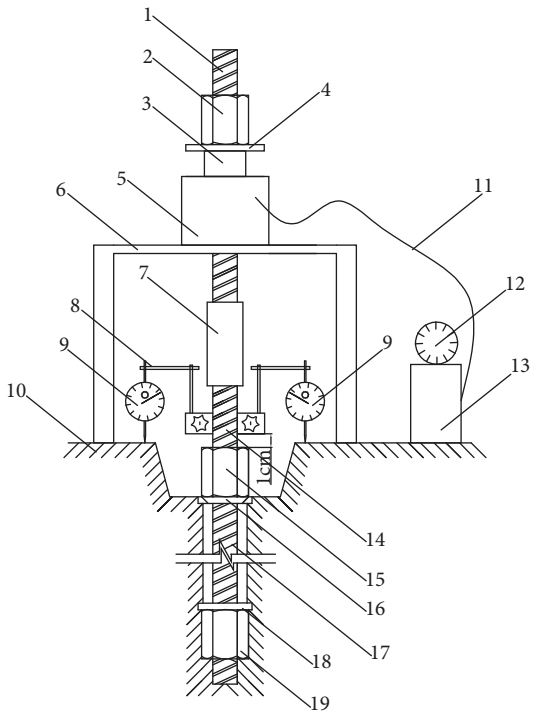

1: connecting screw rod
2: self-locking nut
3: force sensor
4: bearing plate
5: lifting jack
6: reaction frame
7: connecting sleeve
8: magnetic stand
9: dial indicator
10: bridge concrete
11: oil tube
12: oil-pressure gauge
13: oil pump
14: exposed segment of the prestressing tendon
15: anchorage nut
16: cone bore anchor plate
17: tensioning segment of the prestressing tendon
18: circular hole anchor plate
19: nontensioning nut

Figure 7: Schematic view of the tension technology, retraction loss, and tension measurement components.

self-locking nuts, and other components; (2) a force sensor was installed between the self-locking nuts and the lifting jack, and then the magnetic stand and the dial indicator were installed; (3) the oil pump was started, the lifting jack was loaded, the vertical P/S FSSB tension was allowed to reach the predetermined threshold value, the tension was measured with a force sensor, and afterwards, the oil pump's return valve was closed; (4) after the anchorage nut was tightened, the dial indicator value was read and the tension was measured again; lastly (5) the oil pump's return valve was opened, the lifting jack was unloaded, the dial indicator data were recorded again, and then the reaction frame and the self-locking nuts were demolished. The effective tension was calculated according to the study of Zhong et al. [14].

3.2. Signal Testing of the Axial Vibration of FSSB

3.2.1. Test Instrument. The acceleration sensor (Brüel & Kjær 4514-B-001) with a sensitivity of 10 mV/m/s^2 was used, and the analysis and acquisition system of the dynamic signal was the Hi-Techniques Synergy Data Acquisition System.

3.2.2. Test Procedure. (a) The height and mass of the anchorage nut and the mass per unit length of FSSB were measured, and the effective tension was obtained according to the above test scheme (Figure 7) and the study of Zhong et al. [14]; (b) the acceleration sensor was installed on the top anchorage nut surface (Figure 2), the signal analyzer was started, and the sampling frequency was set to 200 kHz; (c) an artificial strike hammer with its head fabricated from chloroprene rubber (shore hardness D60 and weight = 300 g) was used to strike the top part of FSSB (Figure 8); and (d) the acceleration-time histories of axial vibration of the FSSB were obtained first and then the fast Fourier transform (FFT)

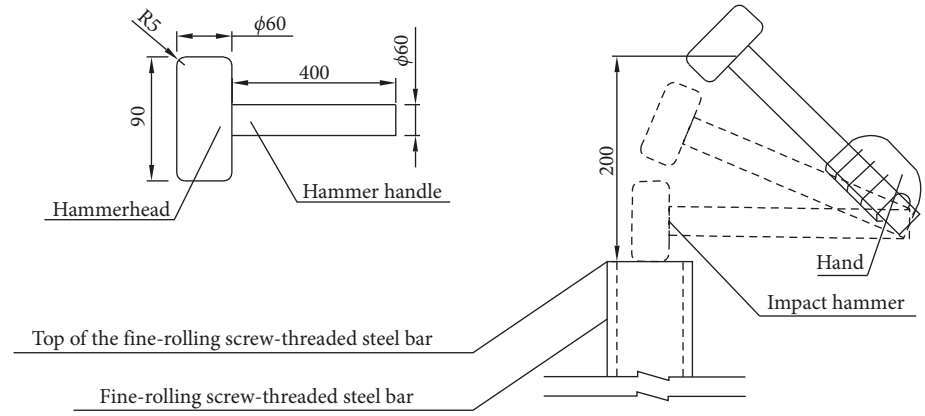

Figure 8: Diagrams showing (a) the impact hammer and (b) shock excitation.

technique was used to convert them into the acceleration-response spectra. The spectra corresponding to the five different effective tensions are shown in Figures 9–13 with the corresponding frequencies listed in Table 1.

3.3. Relationship between the Contact Stiffness and the Effective Tension. The actual vertical P/S FSSB in a bridge is shown in Figure 1, where the bottom anchorage setup is fixed and connected with the concrete girder web. The experimental model shown in Figure 6 differs from that for the actual bridge, where the top and bottom anchorage setups are symmetrical and the same stress state is assumed between them. l_3 in equations (1)–(11) is equal to 1/2 of the length of the tension section in the model, as indicated in Table 1.

According to the anchorage system of FSSB and the relevant parameters indicated in Table 1, the stiffness and mass values of the FSSB and anchorage nut of the test model were computed as summarized in Table 2. Substituting the results from Tables 1 and 2 into equation (19) yields the corresponding effective tensions of 110.8 kN, 210.7 kN, 306.6 kN, 397.9 kN, and 522.6 kN (Table 1). The anchor plate-anchorage nut contact stiffnesses of the experimental model corresponding to the effective tensions are summarized in Table 3. Figure 14 shows the relation between the effective tension and contact stiffness k for the experimental model, which is expressed by the regression equation: effective tension $= 1.63 \times 10^{-5}k - 1038.3$ with $R^2 = 0.9990$ indicating a good linear correlation.

4. Field Test for Assessment of the Contact Stiffness-Effective Tension Relationship

4.1. Engineering Background and Field Test Plan. A field experiment was carried out at Dagutan Bridge in Fujian Province, China, which involves a three-span (66 m + 120 m + 66 m) PC rigid box-girder bridge. The main girder is a single-cell box with variable heights. The vertical P/S FSSB has the nominal diameter of 25 mm, and the control tension for a single steel bar is 327.5 kN. The height of the anchorage nut is 0.065 m. The test instrument and scheme are as described in the above.

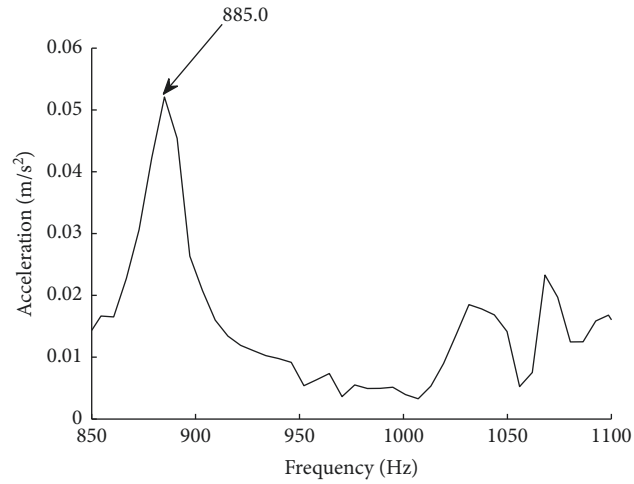

Figure 9: The acceleration-response spectrum corresponding to effective tension = 110.8 kN.

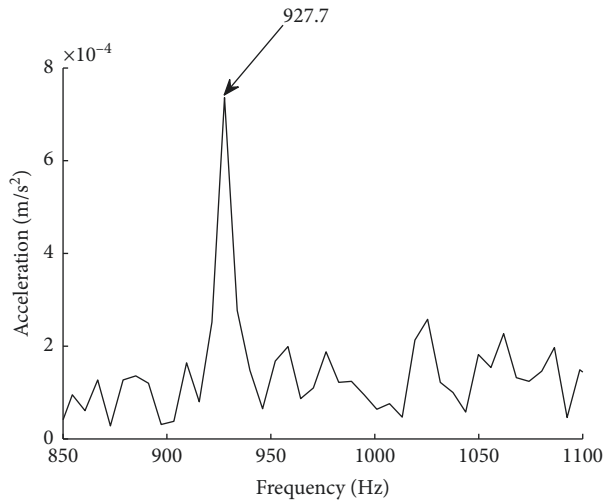

Figure 10: The acceleration-response spectrum corresponding to effective tension = 210.7 kN.

4.2. Results of Frequency Testing and Contact Stiffness Calculation. A field test of 16 P/S tendons was conducted, in which the geometric parameters are listed in Table 4 along

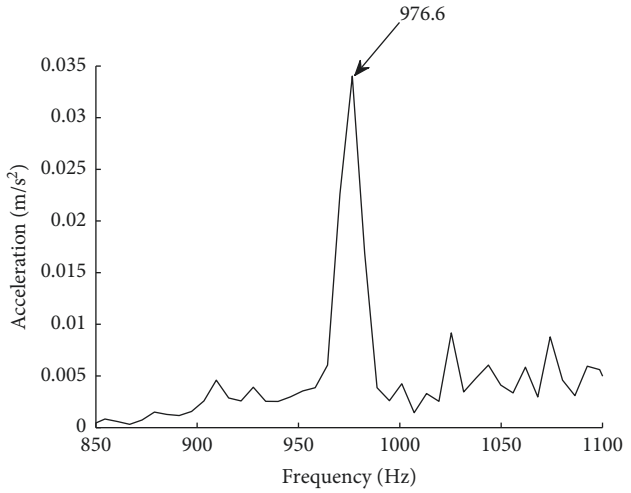

Figure 11: The acceleration-response spectrum corresponding to effective tension = 306.6 kN.

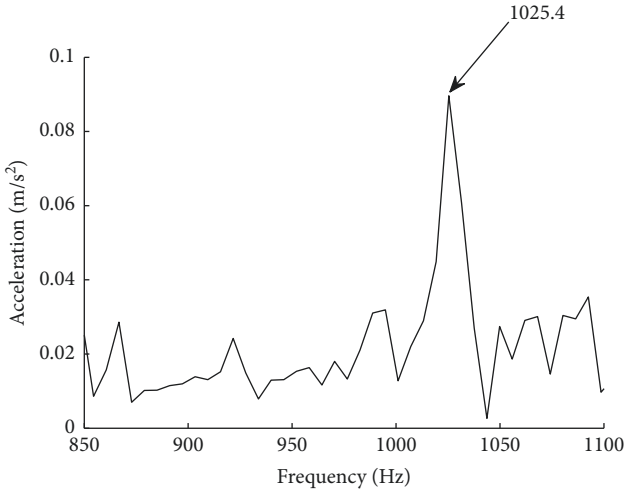

Figure 12: The acceleration-response spectrum corresponding to effective tension = 397.9 kN.

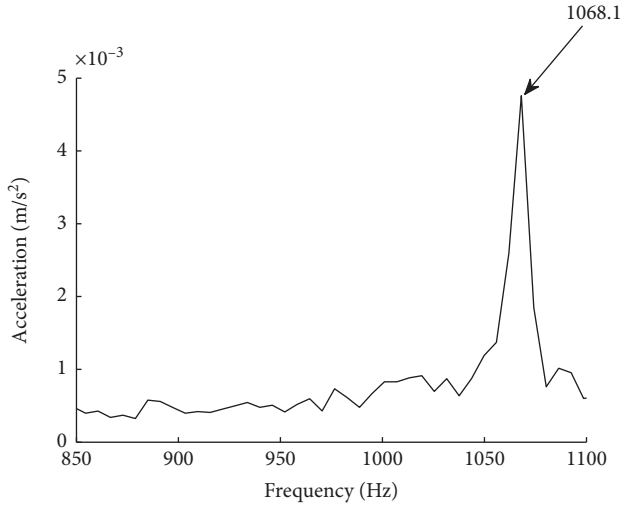

Figure 13: The acceleration-response spectrum corresponding to effective tension = 522.6 kN.

Table 1: The parameters used in the experimental model and the obtained frequencies and effective tensions.

Effective tension (kN)	110.8	210.7	306.6	397.9	522.6
Obtained frequency (Hz)	885.0	927.7	976.6	1025.4	1068.1
l_2 (m)	0.205	0.402	0.135	0.174	0.228
l_3 (m)	3.10/2	3.10/2	3.20/2	3.20/2	3.20/2
$\rho = 7850\ \text{kg/m}^3$; $E = 2.0 \times 10^{11}$ Pa; $A = 0.000804\ \text{m}^2$					

Table 2: Mass and stiffness values of the FSSB and anchorage nut of the test model.

Effective tension (kN)	k_{r1} (N/m)	k_{r2} (N/m)	m_{r1} (kg)	m_{r2} (kg)
110.8	$7.85E+08$	$1.04E+08$	1.311	9.912
210.7	$4.00E+08$	$1.04E+08$	2.571	9.912
306.6	$1.19E+09$	$1.01E+08$	0.863	10.232
397.9	$9.24E+08$	$1.01E+08$	1.113	10.232
522.6	$7.05E+08$	$1.01E+08$	1.458	10.232
$k_s = 9.90E+09$ N/m; $k_t = 4.25E+10$ N/m; $k_{st} = 2.54E+06$ N/m; $m_s = 0.104$ kg; $m_t = 0.438$ kg				

Table 3: Values of contact stiffness k corresponding to the effective tensions of the experimental model.

Effective tension (kN)	110.8	210.7	306.6	397.9	522.6
Contact stiffness, k (N/m)	7.06×10^7	7.66×10^7	8.19×10^7	8.83×10^7	9.57×10^7

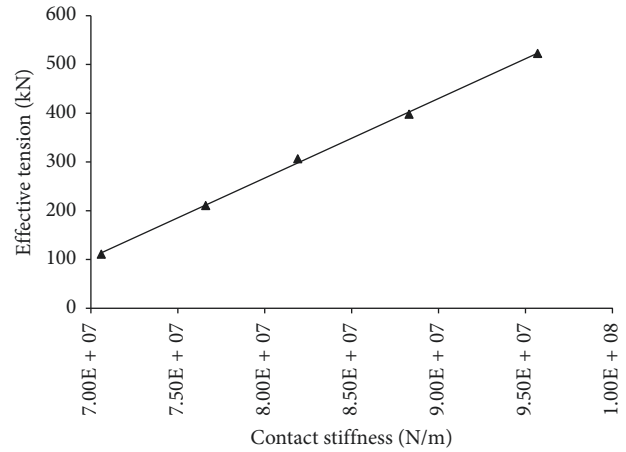

Figure 14: Relation between the contact stiffness k and effective tension for the experimental model.

with the effective tensions and measured frequencies. The computed stiffnesses and masses for the FSSB and anchorage nut based on the field test results are summarized in Table 5. Substituting the results from Tables 4 and 5 into equation (19), the contact stiffnesses are obtained, as shown in Table 6. The relation between the contact stiffness k and effective tension is shown in Figure 15, which is described by the regression equation: effective tension $= 2.68 \times 10^{-6} k - 29.22$

Table 4: The parameters used in and the frequencies measured from the field test.

Number	l_2 (m)	l_3 (m)	Effective tension (kN)	Measured frequency (Hz)
1	0.120	2.517	98.3	498
2	0.123	2.517	196.5	556
3	0.127	2.517	317.6	616
4	0.121	2.517	78.3	478
5	0.124	2.527	220.3	568
6	0.128	2.527	307.6	603
7	0.106	2.527	110.2	514
8	0.109	2.527	196.5	550
9	0.112	2.537	327.6	629
10	0.104	2.537	98.3	493
11	0.108	2.537	210.8	585
12	0.113	2.537	327.6	622
13	0.087	2.547	65.6	488
14	0.161	2.547	196.5	547
15	0.104	2.547	262.1	585
16	0.113	2.547	317.6	605

Table 5: Computed stiffnesses and masses for the FSSB and anchorage nut based on the field test results.

Number	k_{r1} (N/m)	k_{r2} (N/m)	m_{r1} (kg)	m_{r2} (kg)
1	$8.18E+08$	$3.90E+07$	0.469	9.830
2	$7.98E+08$	$3.90E+07$	0.480	9.830
3	$7.73E+08$	$3.90E+07$	0.496	9.830
4	$8.11E+08$	$3.90E+07$	0.473	9.830
5	$7.92E+08$	$3.89E+07$	0.484	9.869
6	$7.67E+08$	$3.89E+07$	0.500	9.869
7	$9.26E+08$	$3.89E+07$	0.414	9.869
8	$9.01E+08$	$3.89E+07$	0.426	9.869
9	$8.77E+08$	$3.87E+07$	0.437	9.908
10	$9.44E+08$	$3.87E+07$	0.406	9.908
11	$9.09E+08$	$3.87E+07$	0.422	9.908
12	$8.69E+08$	$3.87E+07$	0.441	9.908
13	$1.13E+09$	$3.85E+07$	0.340	9.947
14	$6.10E+08$	$3.85E+07$	0.629	9.947
15	$9.44E+08$	$3.85E+07$	0.406	9.947
16	$8.69E+08$	$3.85E+07$	0.441	9.947

$k_s = 6.04E+09$ N/m; $k_t = 2.04E+10$ N/m; $k_{st} = 2.54E+06$ N/m; $m_s = 0.063$ kg; $m_t = 0.210$ kg

with $R^2 = 0.9872$ indicating a good linear correlation. Note that the imperfectly vertical FSSB and uneven contact surface between the anchor plate and anchorage nut in the field contribute to some measurement errors.

5. Application of the Developed Analytical Model for the Axial Vibration of P/S FSSB Anchorage System

The application of the test principle is illustrated in Figure 16. According to the scheme shown in Figure 7, the graded tensioning of P/S FSSB generally started from 200 kN and increased by about 100–200 kN per load level until the design tension was reached. Using this testing procedure (Figure 16), the effective tension in the tensioning section l_3 was calculated based on the study of Zhong et al. [14], the length of the corresponding exposed section l_2 was obtained, the frequency of the exposed section ω was estimated, and the relevant parameters were calculated. The contact stiffness can be calculated by equation (19). The above procedure was repeated, and the test was completed using three additional P/S FSSBs. The relationship between the contact stiffness and effective tension can be described by $T = ak + b$ with a and b being the fitting parameters. This process is shown in Figures 16(a) and 16(b).

Table 6: Contact stiffness k values and effective tensions from the field test.

Number	Effective tension (kN)	Contact stiffness, k (N/m)
1	98.3	$4.68E+07$
2	196.5	$8.59E+07$
3	317.6	$1.30E+08$
4	78.3	$3.43E+07$
5	220.3	$9.45E+07$
6	307.6	$1.21E+08$
7	110.2	$5.72E+07$
8	196.5	$8.16E+07$
9	327.6	$1.35E+08$
10	98.3	$4.37E+07$
11	210.8	$9.59E+07$
12	327.6	$1.35E+08$
13	65.6	$4.05E+07$
14	196.5	$8.52E+07$
15	262.1	$1.11E+08$
16	317.6	$1.22E+08$

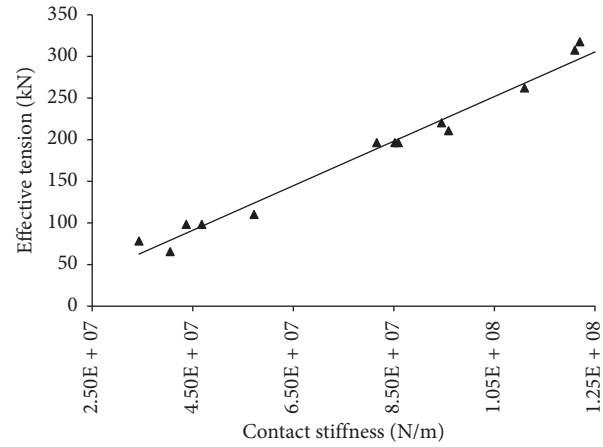

Figure 15: Relation between the contact stiffness k and effective tension from the field test.

After tensioning the vertical P/S FSSB, the natural frequency of axial vibration was tested according to the model shown in Figure 2. By substituting the related parameters into equation (19), the contact stiffness k was obtained. The effective tension T of P/S FSSB was obtained by substituting k into the relation equation between the contact stiffness and effective tension. This process is shown in Figures 16(c) and 16(d).

As seen in Figure 16, the relevant calculation procedure is integrated into the signal analysis device. The fabrication of a specialized testing device (i.e., the tension tester) for

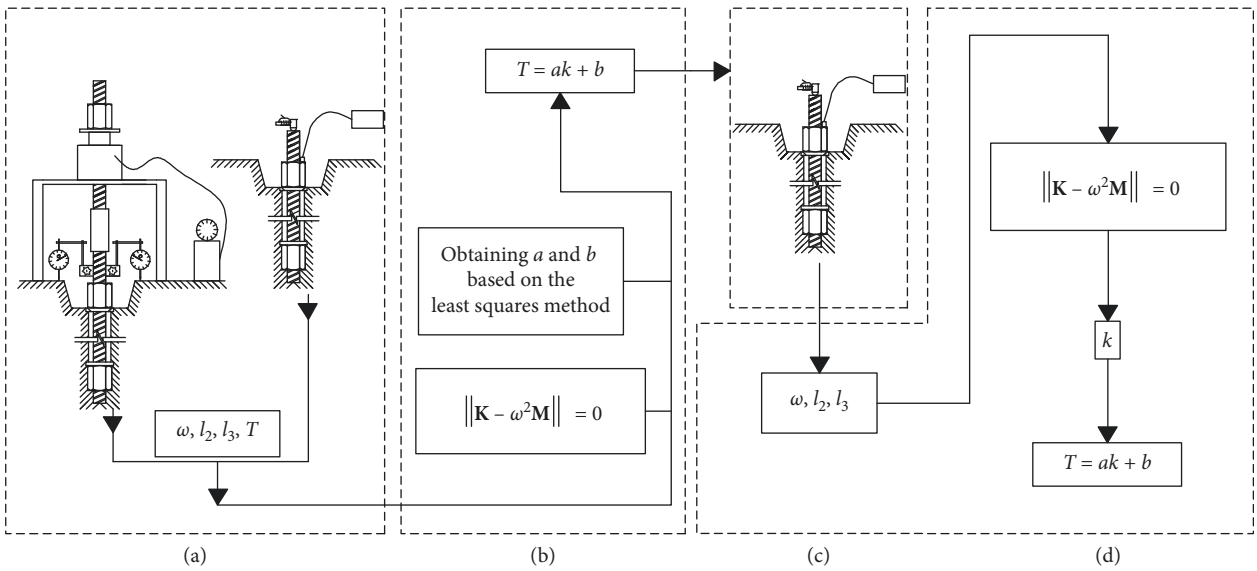

Figure 16: Diagram describing the test principle.

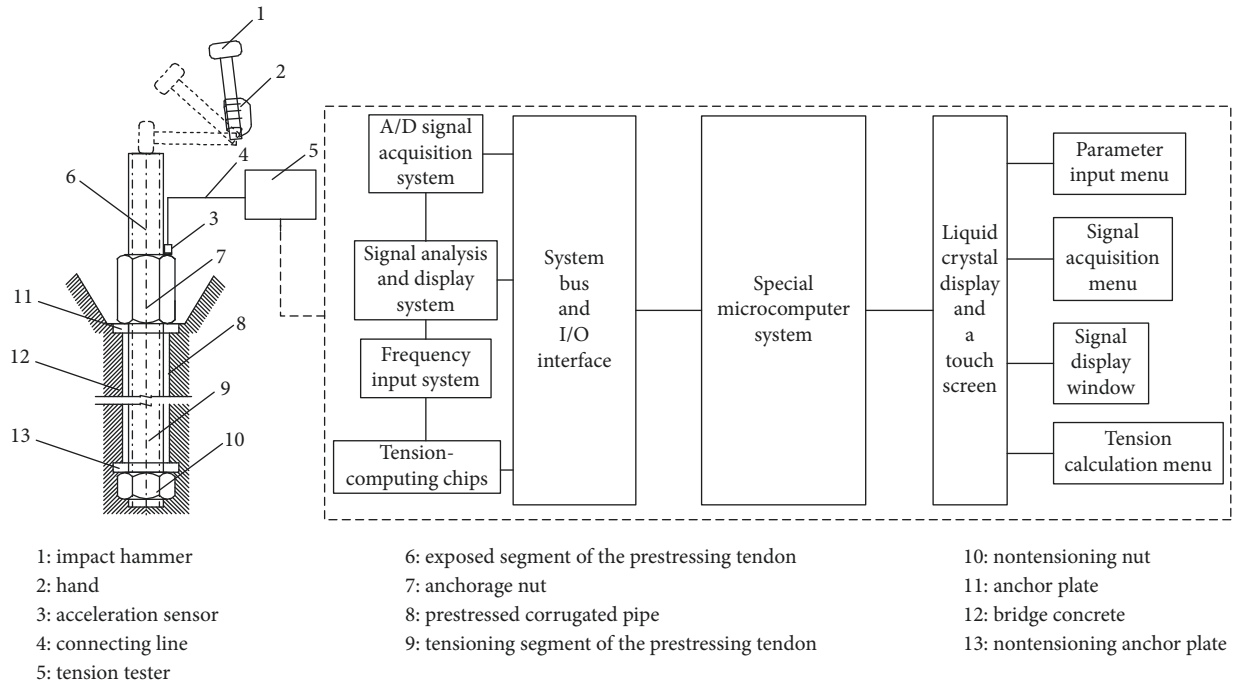

Figure 17: Schematic view of test and block diagram of the device.

estimating the effective tension of P/S FSSBs is presented in Figure 17; this device is comprised of different systems for acquiring and analyzing signals, importing frequencies and calculating tensions. The tension tester controls the main menu of the liquid crystal panel which includes four submenus: the input of the parameter, acquisition of signals, window of the signal display, and module of tension calculation.

6. Conclusions

In this study, the contact between the anchor plate and anchorage nut is represented by a coupling spring whose stiffness is essentially the contact stiffness related to the normal force at the contacting surface, which lifts the usual assumption of fixed connection. The FSSB and nut threads are also connected by a coupling spring whose stiffness is calculated by treating the threads as cantilever components. In this study, an analytical model is proposed for assessing the axial vibration of the P/S FSSB anchorage system. Both model and field tests show that the contact stiffness k between the anchor plate and anchorage nut has a good linear relationship with the effective tension of the P/S FSSB. For practical purposes, a fitted linear equation was derived based on the field test results and is suggested to describe the

contact stiffness k-effective tension relationship of P/S FSSB. Based on the fitted equation and the natural frequency of the axial vibration of P/S FSSB, the contact stiffness k can be determined using the proposed model and then the P/S FSSB's effective tension can be obtained indirectly. The study results show that the effective tension test method is practical and feasible. The developed tension tester has the features of repeated use, fast testing, and minimized impact on the construction; therefore, it is suggested that the proposed method be considered as a nondestructive test for the effective tension of P/S FSSBs.

Data Availability

The data used to support the findings of this study are included within the article.

Conflicts of Interest

The authors declare that they have no conflicts of interest.

Acknowledgments

This work was supported by the National Natural Science Foundation of China (Grant no. 51178183), to which the authors are very grateful.

References

[1] X. Zhong, T. Yang, M. Shen, J. Yu, and X. Xie, "Method for testing the tension of vertical prestressing bars in webs of concrete box girder bridges," *Journal of Bridge Engineering*, vol. 16, no. 3, pp. 438–444, 2011.

[2] A. Majumdar and B. Bhushan, "Fractal model of elastic-plastic contact between rough surfaces," *Journal of Tribology*, vol. 113, no. 1, pp. 1–11, 1991.

[3] H. Tian, B. Li, H. Liu, K. Mao, F. Peng, and X. Huang, "A new method of virtual material hypothesis-based dynamic modeling on fixed joint interface in machine tools," *International Journal of Machine Tools and Manufacture*, vol. 51, no. 3, pp. 239–249, 2011.

[4] P. Liu, H. Zhao, K. Huang, and Q. Chen, "Research on normal contact stiffness of rough surface considering friction based on fractal theory," *Applied Surface Science*, vol. 349, pp. 43–48, 2015.

[5] G.-d. Wang, G.-m. Chen, L.-b. Xu, and Z.-m. Yin, "Axial vibration analysis of the mud recovery line on deepwater riserless mud recovery drilling system," *China Ocean Engineering*, vol. 28, no. 3, pp. 381–390, 2014.

[6] Z. R. Yang, L. U. Kun, Z. S. Rao et al., "Experiment research of axial dynamic vibration absorbers based on magneto-rheological elastomers using for ship shafting," *Journal of Ship Mechanics*, vol. 21, no. 6, pp. 750–760, 2017.

[7] A. Medoued, M. Mordjaoui, Y. Soufi, and D. Sayad, "Induction machine bearing fault diagnosis based on the axial vibration analytic signal," *International Journal of Hydrogen Energy*, vol. 41, no. 29, pp. 12688–12695, 2016.

[8] A. Daabdin, "Static and dynamic analysis of knuckle shape threaded joints," *Mechanism and Machine Theory*, vol. 25, no. 2, pp. 225–232, 1990.

[9] J.-H. Chen, S.-C. Hsieh, and A.-C. Lee, "The failure of threaded fasteners due to vibration," *Proceedings of the Institution of Mechanical Engineers, Part C: Journal of Mechanical Engineering Science*, vol. 219, no. 3, pp. 299–314, 2005.

[10] A. Daadbin and Y. M. Chow, "A theoretical model to study thread loosening," *Mechanism and Machine Theory*, vol. 27, no. 1, pp. 69–74, 1992.

[11] J. Wileman, M. Choudhury, and I. Green, "Computation of member stiffness in bolted connections," *Journal of Mechanical Design*, vol. 113, no. 4, pp. 432–437, 1991.

[12] ISO 6934-5:1991. Steel for the prestressing of concrete--Part 5: Hot-rolled steel bars with or without subsequent processing.

[13] X. Zhong, T. Zhang, C. Zhao, X. Shu, M. Shen, and Y. F. Chen, "New non-destructive dynamic tensile testing of prestressing fine-rolled screw-threaded steel bars," *Engineering Structures*, vol. 182, pp. 153–163, 2019.

[14] X. Zhong, Y. Yan, M. Shen et al., "Research on vertical prestress loss in webs of prestressed concrete box girder due to anchorage slip," *Journal of the China Railway Society*, vol. 36, no. 8, pp. 98–102, 2014.